AIAA JOURNAL
Vol. 33, No. 2, February 1995

Dynamic Stall Control for Advanced Rotorcraft Application

Yung H. Yu,* Soogab Lee,† Kennth W. McAlister,‡ and Chee Tung‡
U.S. Army Aeroflightdynamics Directorate, Moffett Field, California 94035-1000
and
Clin M. Wang§
Georgia Institute of Technology, Atlanta, Georgia 30332

Advanced concepts designed to improve the lift, drag, and pitching moment characteristics of rotor blades have been investigated for the purpose of enhancing rotor maneuver capability. The advantages and disadvantages of these concepts have been evaluated using both computational and experimental means. The concepts that were considered in this study included a leading-edge slat, a deformable leading-edge, and upper-surface blowing. The results show the potential of these concepts for substantially improving the performance of a rotor.

Introduction

THE next generation of rotorcraft will be required to operate at much higher performance levels than in the past, particularly in the areas of nap-of-the-earth (NOE), deep-penetration operations, and air-to-air combat. These new requirements will require highly maneuverable, agile, and survivable rotorcraft, far exceeding the capabilities of those in the current inventory. The objectives of this project include an increase in the maneuverability/agility capability of the helicopter and a reduction in the acoustic detection range.

The single most important element of the rotorcraft for meeting these requirements is the rotor itself, since it is the primary source of lift, control, and speed. At the same time, the rotor is also a major source of acoustically detectable radiation. Among the many factors affecting rotorcraft performance, the aerodynamic characteristics of the rotor system are the most important and are the main subject of this paper.

The maneuvering capability of a rotorcraft can be improved by reducing or suppressing the vibratory loads on the rotor blades caused by aerodynamic separation and stall. This would have the effect of expanding the stall-limiting boundary of the rotor and thereby increase the available load factor in all flight regimes. The conventional way to obtain higher lift is to increase the blade area, however, this usually results in a heavier rotor that is also less efficient. With regard to compressibility effects and acoustic radiation, improvements have been obtained by sweeping, tapering, and thinning the tip region of the rotor blade. As a result, numerous families of airfoils and planform shapes have evolved that offer better advancing-blade characteristics. However, improvements on the retreating-blade side have not been as impressive. One reason for this imbalance may be that design codes are available for treating blades at low angles of attack and high Mach number (characteristic of the advancing side), whereas the design strategy has had to depend heavily on costly empirical studies for blades at high angles of attack and having some amount of separation (characteristic of the retreating side).

Increasing the tip speed of the rotor to achieve a maneuvering advantage may produce a dangerous condition with regard to acoustic detection. Rapid advancements in passive acoustic sensor arrays and advanced signal processing technologies pose a serious threat to the mission effectiveness of Army helicopters. Since the rotor blade generates acoustic radiations that can be easily detected and identified, airfoil and planform shapes must be carefully optimized to reduce the detection range of the rotorcraft.

The requirements for improved maneuverability and reduced susceptibility will clearly demand a substantial growth in the technologies for addressing rotor aerodynamics. New control techniques must be considered, both passive and active, and these must be accompanied by a more thorough physical understanding of these flow phenomena along with substantially improved prediction capabilities. To meet these requirements, computational and experimental efforts have been initiated to evaluate the effectiveness of various concepts. At present these concepts include airfoils with slats and slots, airfoils that deform, and airfoils with flow energizers.

Description of Experiment and Computational Fluid Dynamics Code

The experimental portion of this investigation was conducted in the water tunnel facility at the Aeroflightdynamics Directorate, NASA Ames Research Center. This was a particularly suitable facility because of the ease of obtaining definitive visualizations of the flow and the advantage of examining on-line the unsteady loads on the airfoil. Loads were measured directly by an external apparatus that served as both support and balance for the airfoil.

Two sets of airfoils have been studied so far. The first set was a basic VR-7 airfoil and a VR-7 with the addition of a drooped leading-edge slat. The details of this VR-7 airfoil test were described in Ref. 1. The second set was a basic VR-12 airfoil and a segmented VR-12 with the leading-edge portion extended to form a slat (Fig. 1). The basic VR-7 and VR-12 models both had a chord length of 10 cm, whereas the slat configurations were slightly longer. The test section measured 31 cm (height) by 21 cm (width), and the airfoil was positioned so that it spanned the width of the section to within 0.015 cm on either side. The main body of the airfoil was cast from urethane, and the spar and slats were made from stainless steel.

The spar of the airfoil extended through the test-section windows and was supported by lift and drag transducers on both sides. One end of the spar was adjoined to an instrumented drive shaft through a torsionally stiff coupling so that airfoil incidence could be set and the pitching moment measured. Only quantities relating to the airfoil were electrically instrumented, and these were incidence, lift (both sides), drag (both sides), total pitching moment, and the bearing and seal moments (both sides).

The tunnel was operated at an average dynamic pressure of 0.019 kg/cm^2, which for an ambient temperature of 21°C and an airfoil chord of 10 cm gives a Reynolds number of 200,000. Steady lift, drag, and pitching moment measurements were made from α = 0–30 deg. The unsteady measurements were made with

Received July 27, 1993; revision received May 4, 1994; accepted for publication June 7, 1994.

*Division Chief, Fluid Mechanics Division, NASA Ames Research Center. Associate Fellow AIAA.
†Senior Research Specialist, Sterling Federal Systems. Member AIAA.
‡Research Scientist, Fluid Mechanics Division, NASA Ames Research Center. Member AIAA.
§Senior Research Engineer, School of Aerospace Engineering. Member AIAA.

$\alpha = 15 \text{ deg} + 10 \text{ deg} \sin(2\pi ft)$ and at a reduced frequency k of 0.10. The reduced frequency is related to the oscillating frequency f by the expression $k = \pi fc/v_\infty$, where c is the chord length of the basic airfoil and v_∞ is the freestream velocity.

The computational portion of this investigation involved the ZETA code, which was developed with the vorticity vector as the primary variable. This formulation allowed the unsteady flowfield to be partitioned into its kinematic and kinetic parts. In the kinematic part, the velocity field is related to the vorticity field at any instant of time by the continuity equation and the curl of the velocity. In the kinetic part, the vorticity is computed at each time step by solving the vorticity transport equation. When the flow is turbulent, the kinematic viscosity of the fluid includes the eddy viscosity, and in this case the Baldwin-Lomax model[2] is used. It should be noted that when using the ZETA code the computation of any unsteady flow problem can be confined to the vortical region. This ability offers significant savings in both computer time and storage.

The numerical procedure incorporates a conformal mapping to transfer the physical domain onto a simple region with suitable computational grids. For the two-element airfoil case, the flow outside the airfoil elements is mapped onto the interior domain of two concentric circles. The initial solution starts from a potential flow solution around the solids undergoing an impulsive start motion. A time-marching procedure computes the initial strength of the vortex sheet in the infinitesimally thin layer surrounding the solids. The velocity field corresponding to this initial vorticity field is computed. The vorticity is then diffused from the thin layer and convected away by the velocity field. The process is repeated at each time step until either a converged or a periodic solution is reached. The same procedure can be applied to a single airfoil. A detailed description of the mathematical formulation, conformal transformation, and solution procedure is given in Ref. 3.

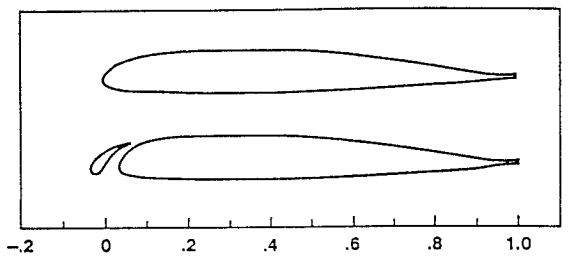

Fig. 1 VR-12 with a leading-edge slat.

The ZETA code was used with suitable modifications to study airfoils with and without slats, an airfoil with a deformable leading edge, and an airfoil with upper-surface blowing. The procedure to solve the deformable leading-edge airfoil includes the conformal transformation of the airfoil coordinates at each time step. As for the airfoil with upper-surface blowing, the wall jet has been numerically simulated by prescribing the tangential velocity distribution at a few grid points on the upper surface of the airfoil. The tangential velocity distribution can be a function of time to simulate an oscillatory blowing condition.

Slatted Airfoils

At this time, experimental data have been obtained for the VR-7 and VR-12 airfoils to determine the effects of a slat configuration for producing high lift in an unsteady environment.[4,5] The measured and calculated loads are for a Reynolds number of 200,000. For the unsteady cases, the pitching motion was $\alpha = 15 \text{ deg} + 10 \text{ deg} \sin(\omega t)$ and the reduced frequency k was 0.10.

The measured steady and unsteady loads for the basic and slatted VR-12 airfoils are shown in Fig. 2. The lift curve for the basic airfoil is fairly linear up to $\alpha = 8$ deg after which the slope decreases due to increasing separation over the aft portion of the airfoil. The increase in separated flow over the upper surface also contributes to an increase in drag. Whereas the pressure on the upper surface

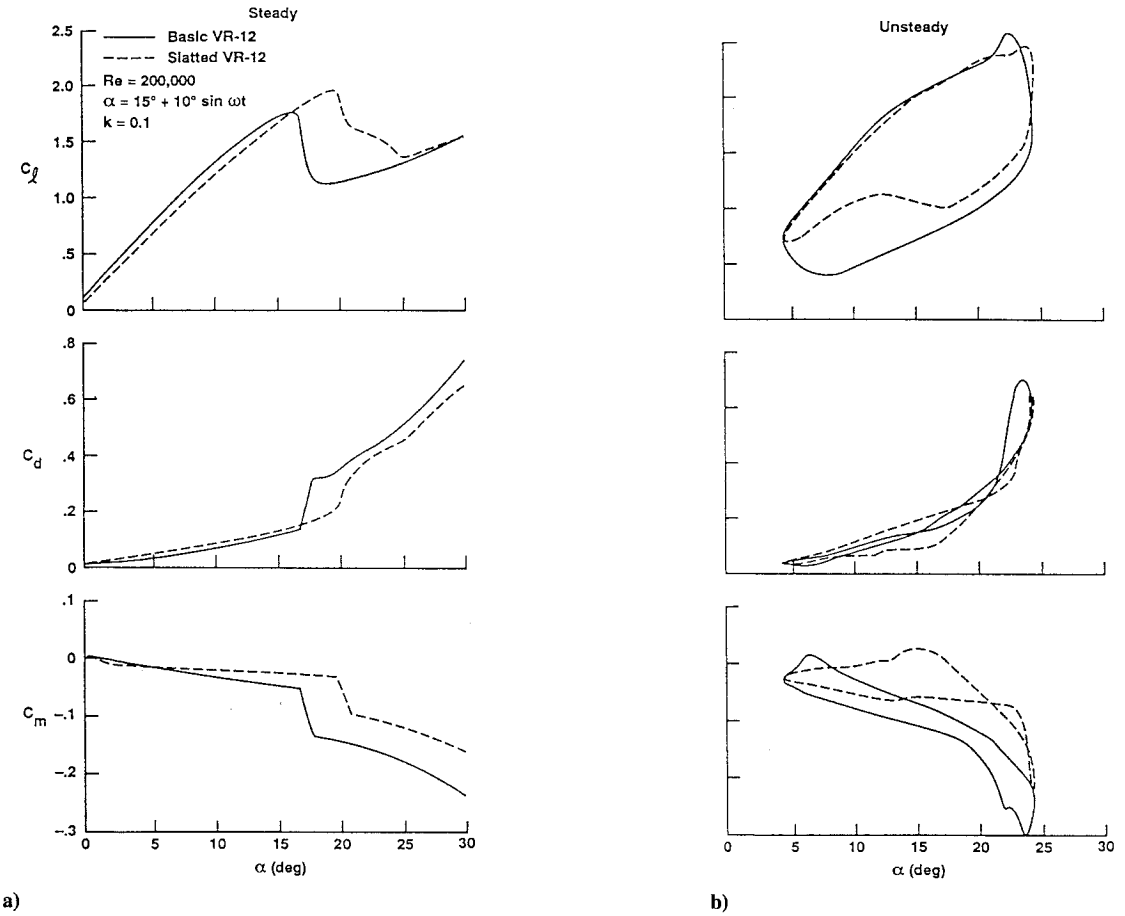

Fig. 2 Measured steady and unsteady loads on the basic and slatted VR-12 airfoils at *Re* = 200,000: a) steady and b) unsteady, α = 15 deg + 10 deg sin(ωt) at k = 0.10.

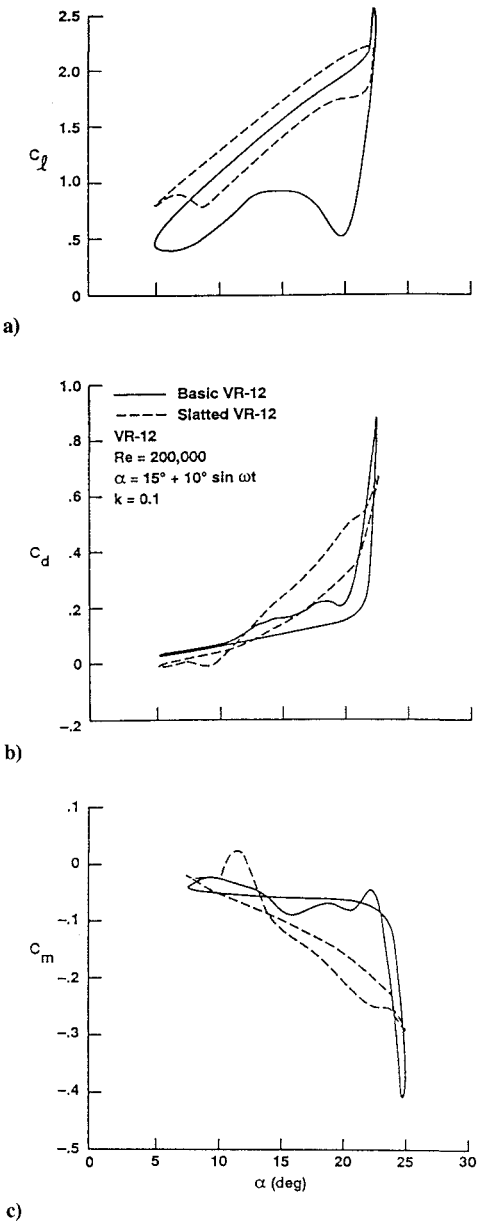

Fig. 3 Calculated unsteady loads on the basic and slatted VR-12 airfoils at Re = 200,000 for α = 15 deg + 10 deg sin(ωt) at k = 0.10.

decreases near the leading edge and increases near the trailing edge (which increases even further due to separation), each invoking a positive moment, the increase in pressure over the lower surface appears to be dominant, resulting in a net shift in the center of pressure toward the trailing edge and an increase in the magnitude of the pitching moment. At about α = 18 deg an abrupt change in all of the loads occurs, signaling that the airfoil has stalled. The fact that the VR-12 has an upper surface that is much flatter than the VR-7 airfoil may account for the significantly more abrupt stall than was observed in the latter case.

The steady loads on the slatted airfoil exhibit a slight deviation in the pitching moment near α = 0 deg, which is most likely due to the movement of the stagnation point around the leading edge of the slat and a sudden increase in the flow between the slat and the main element. Apart from the region around α = 0 deg, the lift varies linearly with α until reaching α = 12 deg. All of the loads show a steady increase with angle of attack until reaching around α = 20 deg, at which time the airfoil experiences an abrupt stall. Visualizations of the flow showed that the boundary layer is considerably thicker at α = 15 deg, and that some amount of separated flow was present over the aft portion of the airfoil. This condition no doubt accounts for the decrease in the slope of the lift curve. The confluent boundary layers from the slat and the main element remain well defined over the forward portion of the airfoil until α = 20 deg. An additional increase of only 1 deg causes the flow to completely separate from the main element. At this angle the flow over a major portion of the slat has also separated, however the slat does not fully separate until α = 25 deg.

Considering the unsteady results on the basic airfoil when $\dot{\alpha} > 0$, a modest amount of separation was observed to occur near the trailing edge as the angle of attack of the airfoil moves past α = 8 deg. Around α = 15 deg the separation point on the upper surface moves up the airfoil and causes the slope of the lift curve to noticeably decrease. At about α = 21 deg a vortex forms near the leading edge. After reaching α = 22 deg the flow is fully separated from the upper surface, and the stall vortex has moved halfway down the airfoil. At this point the lift, drag, and pitching moment are all rapidly increasing in magnitude. At α = 25 deg, the vortex moves into the wake and all of the loads quickly decrease in magnitude. When $\dot{\alpha} < 0$ the reattachment point slowly moves away from the leading edge and over the upper surface of the airfoil. The hump in the pitching moment curve around α = 6 deg corresponds to the movement of the reattachment point past the quarter-chord pitch axis.

The results for the slatted airfoil show a large hysteresis in the lift. The rapid increase in the drag and pitching moment near α = 24 deg indicates that the slat does not prevent the airfoil from stalling over this α range. For $\dot{\alpha} > 0$ the flow is attached, and the lift smoothly increases with no appreciable separation on the airfoil as the angle of attack moves past α = 15 deg. At α = 22 deg the separation point on the upper surface has moved up to about x/c = 0.6 and is accompanied by a noticeable decline in the slope of the lift curve. At α = 25 deg the flow has fully separated, and the drag and pitching moment loads are near their maximum values. Over the remainder of the cycle the reattachment point slowly moves toward the trailing edge. A brief positive-going surge in the moment curve occurs at α = 15 deg when the reattachment point moves past the quarter-chord pitch axis.

The calculated results using the ZETA code are shown in Fig. 3 for the unsteady case. The solution for the basic airfoil shows that

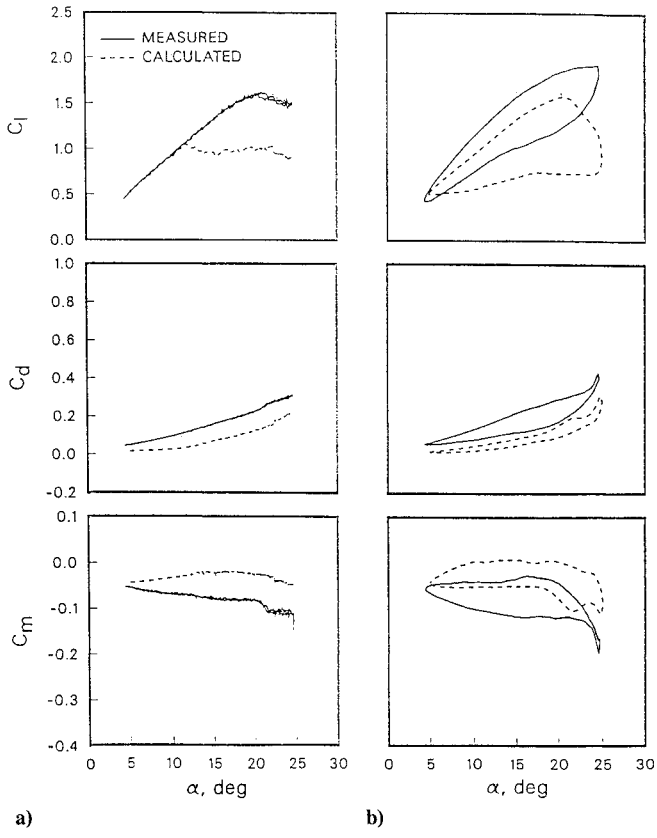

Fig. 4 Comparison for measured quasistatic and dynamic loads of the drooped VR-12 (case 2513) airfoil at conditions of Re = 200,000, α = 15 deg + 10 deg sin(ωt): a) k = 0.0026 and b) k = 0.10.

a strong stall vortex is present, as indicated by the sudden increase in all of the loads near $\alpha = 25$ deg. The undulations in the pitching moment curve during $\dot{\alpha} < 0$ suggests that there are multiple secondary vortices forming during the reattachment phase. The solution for the slatted airfoil is quite different. Judging by the modest hysteresis amplitude in the lift curve and the absence of any surge in the lift near α_{max}, a stall vortex does not appear to form in this case. Although the peak values of the drag and pitching moment are lower than for the basic airfoil, these loads are still larger than desired. When compared with the measured results, the calculated peak loads for the slatted airfoil differ from the basic airfoil by about the same amount. Overall, the calculations suggest that the performance of the slatted airfoil is superior to the basic airfoil. Quantitatively, there are some differences between the measured and the calculated results. The calculated lift is higher and the hysteresis amplitude is less than what was measured. In addition, the calculated drag appears to increase at much lower values of α, indicating that more of the boundary layer may be separated than what was actually present in the measured data. Finally, the calculated variation of the pitching moment with α over a majority of the cycle for the basic airfoil is much flatter than for the slatted airfoil, whereas the measured results show just the opposite behavior.

In summary, it appears that a significant improvement in performance can be achieved with a slat configuration. The superior behavior of the slatted VR-7 airfoil compared with that of the VR-12 may indicate 1) the need to rotate and droop the slat rather than to simply extend the slat element forward and 2) the importance of curvature on the upper surface of the main element for some distance behind the slat.

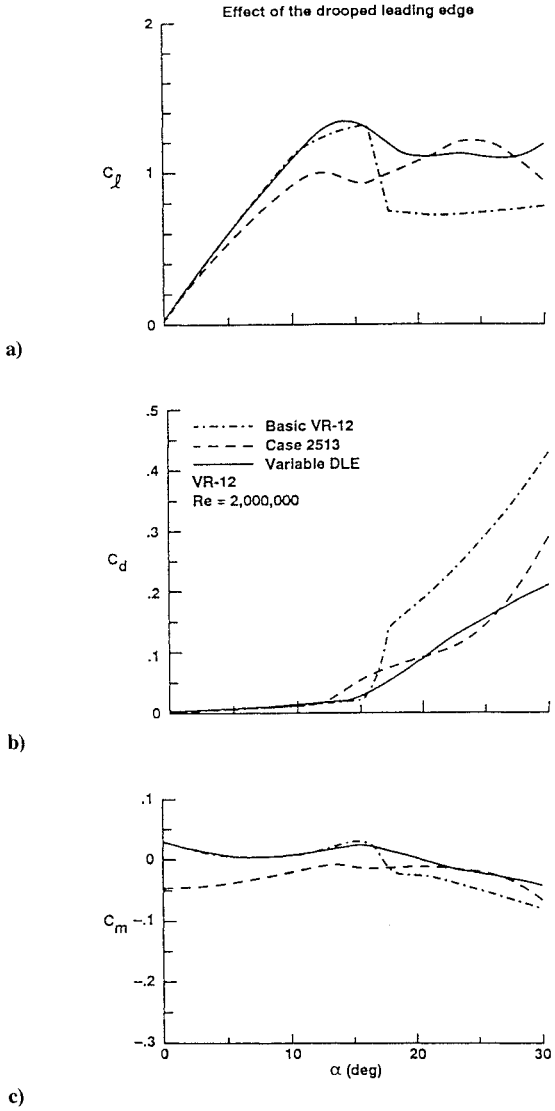

Fig. 5 Calculated steady loads on the basic VR-12 airfoil, the drooped VR-12 (case 2513) airfoil, and the variable droop leading-edge airfoil at $Re = 2 \times 10^6$.

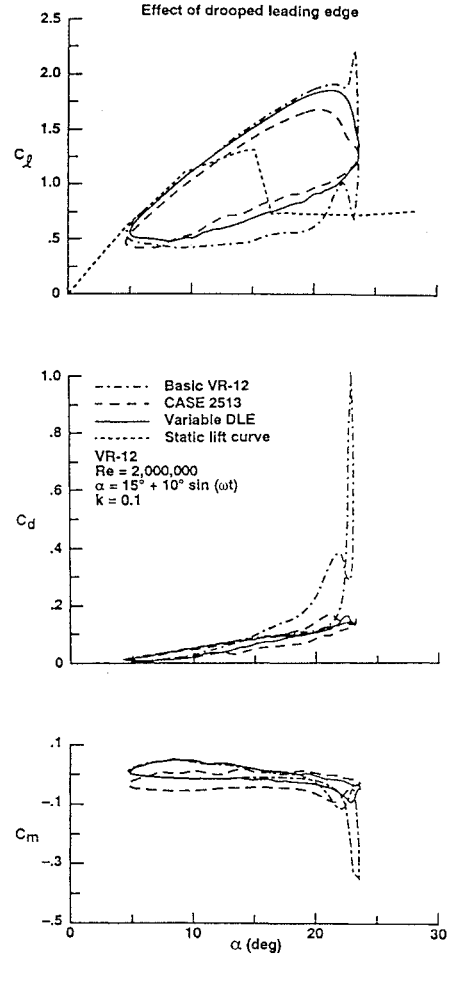

Fig. 6 Calculated dynamic loads on the basic VR-12 airfoil, the drooped VR-12 (case 2513) airfoil, and the variable droop leading-edge airfoil at $Re = 2 \times 10^6$, $\alpha = 15$ deg + 10 deg sin(ωt), and $k = 0.1$.

Deformable Airfoils

The deformable leading-edge (DLE) concept for delaying or suppressing dynamic stall has been approached by drooping the forward portion of the airfoil at high angles of attack so that the flow can easily pass around the leading edge. There are two geometric parameters for specifying the drooped leading edge; one is the center of rotation and the other is the droop angle. In our notation, for example, the case 2513 means that the center of rotation is located at 25% of the chord and the droop angle is 13 deg. Calculations of the static and dynamic performance of several fixed drooped airfoil configurations were made with the center of rotation and the drooped angle as parameters. These results show case 2513 to have the best pitching moment. The test and calculated results for case 2513 (fixed drooped angle) with a Reynolds number of 200,000 and reduced frequencies k of 0.0026 and 0.1 are presented here.

A comparison between experimental and computational results for a very slow oscillation $k = 0.0026$ (quasisteady) is shown in Fig. 4a. The measured lift coefficient shows no stall until the angle of attack reaches about 20 deg. However, the code shows that the drooped airfoil has an earlier stall at an angle about 12 deg. The calculated drag and pitching moment show the general trend as the measured values. One place that is easy to blame for the discrepancy is the turbulence modeling. Needless to say, turbulence modeling should be improved to simulate the dynamic stall phenomenon accurately. Unfortunately none of the eddy-viscosity turbulence models

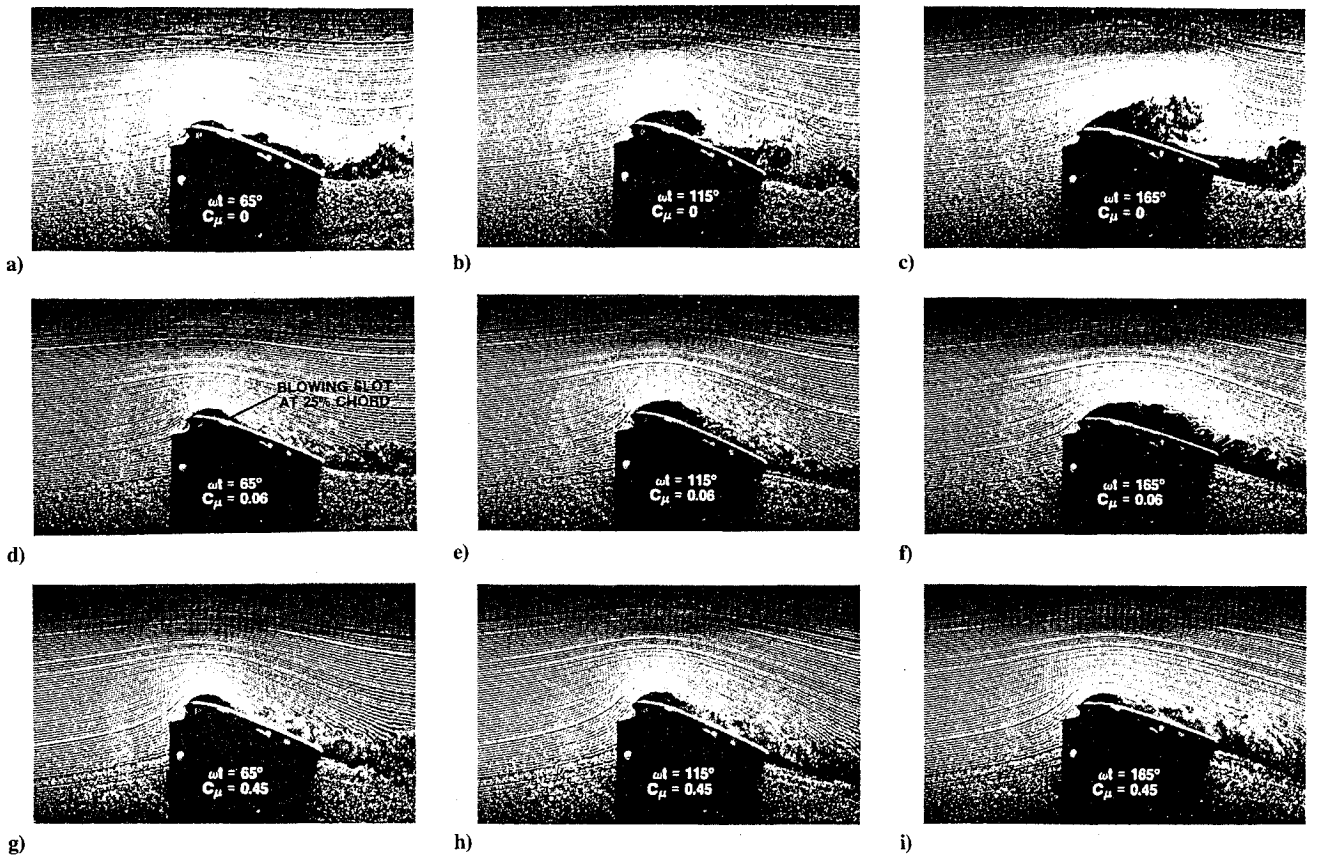

Fig. 7 Exploratory study by McAlister and Carr on the effect of upper-surface blowing on dynamic stall; test conducted in water tunnel on NACA 0012 airfoil at Re = 30,000 with α = 10 deg + 10 deg sin(ωt) and k = 0.49.

(from algebraic to two-equation), at the present stage, can predict separation accurately in all cases.[6,7] Another possible reason for the discrepancy is the transition modeling. This is particularly true if the Reynolds number is below 500,000 and a separation is followed by a reattachment of the flow, forming what is known as a separation bubble. This phenomenon can not be properly simulated without a transition model which is able to provide the transition onset and length accurately.[8–10]

The dynamic measurements of the drooped VR-12 (case 2513) airfoil are compared with the computed results in Fig. 4b. In the experiment, it shows a significant decrease in lift hysteresis with about a 40% reduction in the magnitude of the drag and pitching moment as compared with the basic VR-12 airfoil in Fig. 2. Since the dynamic stall vortex does not appear to form on the drooped airfoil, there is no sudden increase in lift that experienced by the basic airfoil. The gain in overall lift (integrated over the cycle of oscillation) was achieved mainly on the downstroke since the stall is delayed and attenuated by drooping the leading edge. On the other hand, the computed results predicted an earlier stall and, consequently, overestimated the drag and pitching moments reductions.

The predictions for the airfoil with a fixed droop angle show a limited success as compared to the test data. Nevertheless, the computational fluid dynamics (CFD) code is utilized to assess the effect of the variable-droop leading-edge concept (VDLE). For the VDLE case, the droop angle θ vs the angle of attack α was selected as follows:

$$\theta = \alpha - 13.0 \quad \text{for} \quad \alpha \geq 13.0$$

$$\theta = 0.0 \quad \text{for} \quad \alpha < 13.0$$

The results for a Reynolds number of 2×10^6 and a reduced frequency k of 0.1 are presented here. Additional results are reported in Ref. 11.

The calculated static lift, drag, and pitching moment were calculated at discrete angles of attack from 0 to 30 deg. The load characteristics of the basic VR-12 airfoil, a drooped VR-12 (case 2513), and a VDLE case are compared in Fig. 5. The lift coefficient of the no-droop case simply increases until α = 15 deg. Slightly above α = 16 deg, the airfoil stalls, causing C_l to drop to a minimum value. Above α = 18 deg, C_l remains almost constant. For case 2513, the airfoil also experiences a stall at α = 13 deg, but the magnitude is much smaller since the stall occurs near the trailing edge instead of the leading edge. This airfoil eventually encounters a leading-edge stall at α = 25 deg and the lift drops quickly. The performance of the VDLE is much better than the previous two cases. A comparison of the drag in these three cases clearly shows that the static stall is delayed on the drooped airfoil. The variation of the pitching moment with angle of attack is also reduced.

The pitch axis for both the basic and the drooped (case 2513 or VDLE) VR12 airfoils is at the quarter chord of the main airfoil. The pitching motion is described by α = 15 deg + 10 deg sin(ωt), which means that the airfoil oscillates from α = 5 to α = 25 deg. The calculated hysteresis loops for the lift, drag, and pitching moment coefficients are shown in Fig. 6. For the basic VR12 airfoil, the dynamic stall effect is quite evident. The dynamic lift curve is much higher than the static lift curve on the upstroke because the boundary layer on the upper surface near the nose tends to be compressed as the airfoil pitches up, consequently delaying the leading-edge separation. At α = 23 deg, there is a rapid increase in lift that accompanies the formation of the leading-edge vortex, which then suddenly drops as the vortex is shed downstream. When the vortex is detached from the airfoil, the airfoil experiences a large increase in the drag and nosedown pitching moment with a drastic loss of lift, as seen in Fig. 6. The drooped VR12 (case 2513) airfoil experiences a separation only near the trailing edge. The lift hysteresis loop in this case shows that deep dynamic stall is not encountered. Consequently, both the drag and the moment hysteresis loops do not experience any abrupt increases, as compared with the basic VR-12 airfoil. The hysteresis loop of the lift in the VDLE case shows ever better performance than does the 2513 case. It maintains almost the same lift as the basic airfoil up to α = 23 deg on the upstroke and then experiences a stall with a smaller hysteresis amplitude. After the stall, the lift curve of the VDLE case on the downstroke closely

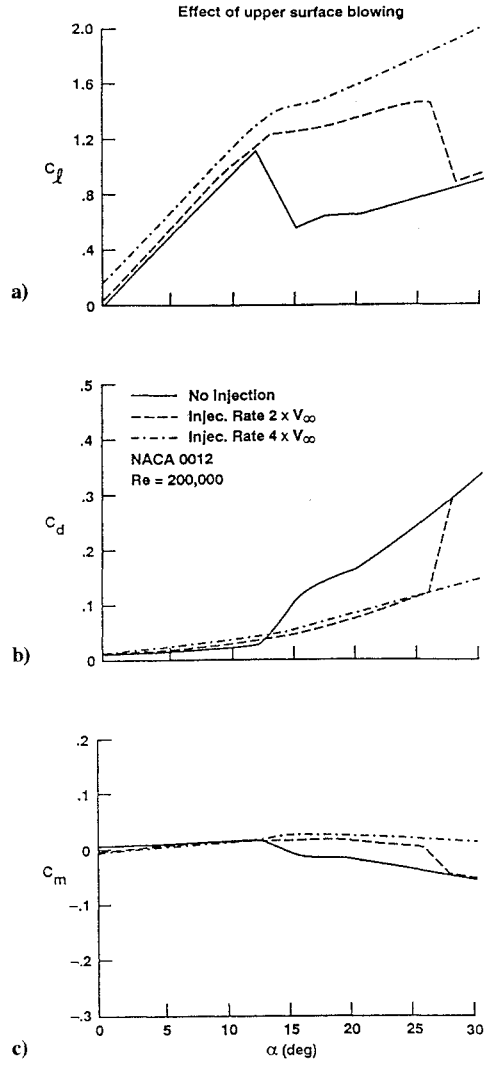

Fig. 8 Calculated steady loads on the NACA 0012 airfoil with and without upper-surface blowing at Re = 200,000.

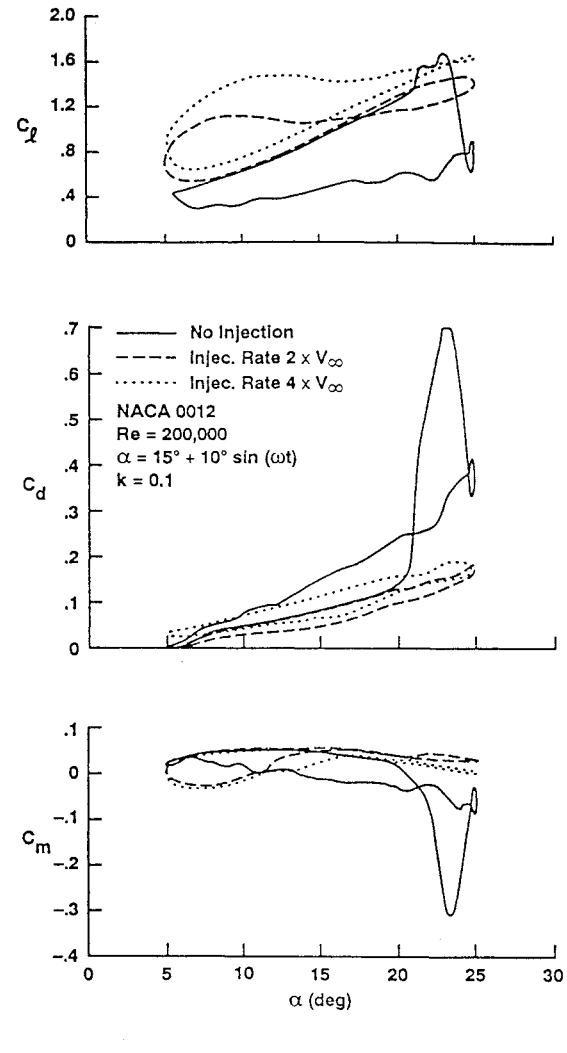

Fig. 9 Calculated dynamic loads on the NACA 0012 airfoil with and without upper-surface blowing at Re = 200,000 with α = 15 deg + 10 deg sin(ωt) and k = 0.10.

follows the 2513 case. The hysteresis loops of the drag and pitching moment in the VDLE case does not show any peak, whereas the basic case shows a large peak.

Surface-Blown Airfoils

The concept of upper-surface blowing has been tested in the Army's water tunnel at NASA Ames Research Center in the early 1980s. The flow visualization from the test is very encouraging. Figure 7 shows a NACA 0012 airfoil oscillating with a pitching motion of $\alpha = 10 \text{ deg} + 10 \text{ deg} \sin(2\pi f t)$, a reduced frequency k of 0.49, and a Reynolds number of 30,000. The tangential blowing slot was located at the quarter chord on the upper surface of the airfoil. Three blowing rates of $C_\mu = 0.0, 0.06$, and 0.45 were tested. The case of $C_\mu = 0.0$ corresponds to no blowing on the upper surface. Without blowing, the airfoil encountered dynamic stall. At the moderate blowing rate of $C_\mu = 0.06$, the leading-edge vortex was modified, and the vortical region associated with the vortex was reduced. For the large blowing rate of $C_\mu = 0.45$, the location of the leading-edge vortex remained stationary during the complete cycle.

The ZETA code has been modified to include upper-surface blowing. As mentioned in the previous section, the upper-surface blowing has been simulated by prescribing a nonzero tangential velocity on part of the upper-surface. In the present numerical study, the constant nonzero tangential velocity is prescribed at 5 grid points near the quarter chord on the computational grid with 80 grid spacings in the airfoil circumferential direction. The magnitude of the tangential velocity was chosen to be two and four times the freestream velocity. These were considered to be typical values for the study of circulation control airfoils (e.g., Ref. 12). The present numerical results are for a NACA 0012 airfoil at Reynolds number of 200,000. The flow is assumed to be fully turbulent.

Figure 8 shows the variation of the lift coefficient with respect to the angle of attack. The two cases for simulating the surface blowing are presented in contrast to the case of no blowing. Without blowing, the computational results show that the airfoil stalls at approximately 13 deg. For the case of injection at twice the freestream velocity, the blowing delays the stall until about 25 deg and shows a moderate amount of increase in lift. The case with four times the freestream velocity does not show any sign of stall even at 30 deg, and the lift is higher compared to the case with twice the freestream velocity. The lift curves for the three cases have almost the same slope in the region of small to moderate angles of attack. The slope for the two blowing cases decreases in the region of moderate angles of attack. This is attributed to a moderate flow separation region on the upper surface. In this angle-of-attack range, the flow patterns are similar since the separation point is prevented from moving upstream by the flow injection. The drag and moment coefficients are shown in Fig. 8. The blowing delays the stall and, therefore, reduces the drag at higher angles of attack compared to the case of no blowing. The higher drag at lower angles of attack for the blowing cases is caused by the low value of the surface pressure associated with the flow injection.

Figure 9 shows the loads hysteresis of the oscillating airfoil at a reduced frequency of 0.1 for pitching motions described by $\alpha = 15 \text{ deg} + 10 \text{ deg} \sin(2\pi f t)$. The lift coefficient for the case without blowing exhibits typical deep dynamic stall characteristics.

During the airfoil upstroke, the lift increases almost linearly until reaching an angle of attack of 20 deg, when a sudden surge in the lift occurs. This surge in the lift is closely related to the formation of a dynamic stall vortex. This high lift region persists while the angle of attack increases about another 3 deg, and then starts to drop rapidly. The high lift is caused by the combination of the growth and the downstream movement of the dynamic stall vortex. The movement of the dynamic stall vortex, however, causes the moment stall as shown in Fig. 9. The low value of the surface pressure associated with the stall vortex also causes the drag to be high during this period. The drastic drop in lift is caused by the shedding of the stall vortex into the wake. During this process, the moment coefficient recovers and the drag coefficient drops. The lift then rises slightly before the airfoil reaches the maximum angle of attack and then drops again to reach an almost constant level during the airfoil downstroke. The slight rise and drop of the lift is attributable to a dynamic stall vortex on the airfoil upper surface.

The lift hysteresis for the blowing cases show significant differences compared to the no-blowing case. From the computed streamlines, not shown here, there is no dynamic stall vortex formed in the blowing cases. The flow injection on the surface prevents the separation point from moving upstream. The nearly constant lift during the large part of the airfoil downstroke suggests that the flows have very similar characteristics during this period. For the high blowing case, the higher lift during the downstroke compared with the lift during the upstroke is caused by a moderate but stable separation region attached to the aft part of the airfoil upper surface. The low pressure in this region contributes more to the lift than would be the case when there is either less separation or no separation at all. The injection in both the blowing cases eliminates the moment stall completely.

Concluding Remarks

The demand for higher performance and reduced susceptibility require substantial improvements in the rotorcraft technology base. Incremental contributions are not sufficient and, instead, we must look to unconventional means for meeting this new challenge. This means that we must look for major breakthroughs in aerodynamic technology and be more receptive to new and innovative concepts.

Therefore, several new and innovative flow control concepts such as slatted, deformable, and surface blown airfoils were examined. The effectiveness of these concepts was also evaluated using computational and experimental methods. Each concept appears to show encouraging results. The slatted airfoil configuration can achieve a significant improvement in the aerodynamic characteristics with an optimum slat location. For deformable airfoils, drooping the leading edge during a pitch oscillation can enhance the airfoil in lift, drag, and pitching moment. In particular, the experiment shows a drastic decrease in lift hystersis and in the magnitude of the drag and pitching moment compared with the basic airfoil. Based on the CFD computations these performances can be further enhanced by actively deforming the leading edge during the oscillatory motion. The experimental results show that the upper-surface blowing concept delays the dynamic stall phenomenon by trapping the stall vortex. Further study with the computational method indicates that a stall vortex does not form on the airfoil when there is upper-surface blowing at the quarter chord. This concept can be improved by adding various active flow energizing techniques such as oscillating flaperons or acoustic waves.

Although each concept seems to have some effectiveness in delaying dynamic stall, the application of these concepts to rotorcraft requires further tests on the effects of high Mach numbers and high Reynolds numbers.

References

[1]Tung, C., McAlister, K. W., and Wang, C. M., " Unsteady Aerodynamic Behavior of an Airfoil With and Without a Slat," *Computers in Fluids*, Vol. 22, No. 415, 1993, pp. 529–547.

[2]Baldwin, B., and Lomax, H., "Thin Layer Approximation and Algebraic Model for Separated Turbulent Flows," AIAA Paper 78-0257, Jan. 1978.

[3]Wang, C. M., Wu, J. C., and Tung, C., "A Numerical Study of General Viscous Flows Around Multi-Element Airfoils," AIAA Paper 90-0572, Jan. 1990.

[4]McAlister, K. W., and Tung, C., "Suppression of Dynamic Stall with a Leading-Edge Slat on a VR-7 Airfoil," NASA-TP 3357, March 1993.

[5]Plantin De Hugues, P., McAlister, K. W., and Tung, C., "Effect of an Extendable Slat on the Stall Behavior of a VR-12 Airfoil," NASA-TP 3407, Sept. 1993.

[6]Menter, F. R., "Performance of Popular Turbulence Models for Attached and Separated Adverse Pressure Gradient Flows," AIAA Paper 91-1784, June 1991.

[7]Clarkson, J. D., Ekaterinaris, J. A., and Platzer, M. F., "Computational Investigation of Airfoil Stall Flutter," *Unsteady Aerodynamics, Aeroacoustics and Aeroelasticity of Turbomachines and Propellers*, edited by H. M. Atassi, Springer-Verlag, 1991, pp. 415–432.

[8]Walker, G. J., Subroto, P. H., and Platzer, M. F., "Transition Modeling Effects on Viscous/Inviscid Interaction Analysis of Low Reynolds Number Airfoil Flows Involving Laminar Separation Bubbles," American Society of Mechanical Engineers Gas Turbine Congress, ASME 88-GT-32, 1988.

[9]Ekaterinaris, J. A., and Menter, F. R., "Computation of Separated and Unsteady Flows with One- and Two-Equation Turbulence Models," AIAA Paper 94-0190, Jan. 1994.

[10]Ekaterinaris, J. A., Chandrasekhara, M. S., and Platzer, M. F., "Analysis of Low Reynolds Number Airfoil Flows," AIAA Paper 94-0534, Jan. 1994.

[11]Lee, S., McAlister, K. W., and Tung, C., "Characteristics of a Deformable Leading-Edge for High Performance Helicopter Rotor," AIAA Paper 93-3526, Aug. 1993.

[12]Shrewsbury, G. D., "Evaluation of Research Circulation Control Airfoil Using Navier-Stokes Methods," NASA-CP 2432, 1986.